ELSEVIER

Journal of Chromatography A, 962 (2002) 57–67

JOURNAL OF CHROMATOGRAPHY A

www.elsevier.com/locate/chroma

Application of the general rate model and the generalized Maxwell–Stefan equation to the study of the mass transfer kinetics of a pair of enantiomers

Krzysztof Kaczmarski[a,b,1], Alberto Cavazzini[a,b,2], Paweł Szabelski[a,b,3], Dongmei Zhou[a,b], Xiaoda Liu[a,b], Georges Guiochon[a,b,*]

[a]*Department of Chemistry, The University of Tennessee, Knoxville, TN 37996-1600, USA*
[b]*Division of Chemical and Analytical Sciences, Oak Ridge National Laboratory, Oak Ridge, TN 37831-6120, USA*

Received 29 October 2001; received in revised form 6 May 2002; accepted 8 May 2002

Abstract

The general rate model of chromatography can be coupled with the generalized Maxwell–Stefan equation that describes the surface diffusion flux. The resulting model is useful to describe the behavior of two enantiomers during their separation on chiral phases, cases in which the mass transfer kinetics is known to be sluggish. A case in point is the modeling of the elution profiles of the racemic mixture of the two enantiomers of 1-phenyl-1-propanol on cellulose tribenzoate coated on silica, a popular chiral stationary phase. The competitive equilibrium isotherm behavior of the two enantiomers on the chiral stationary phase was described using the competitive Tóth isotherm model. An excellent agreement between the experimental and the calculated profiles was observed in the whole range of experimental conditions investigated, at low and high column loadings.

Keywords: Enantiomeric separation; General rate model; Generalized Maxwell–Stefan equation; Kinetic studies

1. Introduction

The production of very pure enantiomers of synthons (synthesis intermediates) has recently become a most important issue in the pharmaceutical industry. Although, in principle at least, this production can be performed by the stereoselective synthesis of the desired enantiomer, such syntheses are most difficult and expensive or are rarely selective enough to afford the required enantiomeric purity. The extraction, separation, and purification of the desired enantiomer from the synthesis products become then necessary. Preparative chiral chromatography is the most powerful and flexible method available for these operations [1,2]. It has significant advantages over other available separation techniques (e.g., crystallization) to produce optically pure compounds.

*Corresponding author. Tel.: +1-865-9740-733; fax: +1-865-9742-667.

E-mail address: guiochon@utk.edu (G. Guiochon).

[1]On leave from Faculty of Chemistry, Rzeszów University of Technology, W. Pola 2 Street, 35-959, Rzeszów, Poland.

[2]Present address: University of Ferrara, Ferrara, Italy.

[3]Present address: Department of Theoretical Chemistry, Maria-Curie Sklodowska University, Pl. M.C. Sklodowskiej 3, 20-031 Lublin, Poland.

0021-9673/02/$ – see front matter
PII: S0021-9673(02)00585-X

In a separate report [3], we investigated the thermodynamics and the mass transfer kinetics of the chiral separation of the racemic mixture of 1-phenyl-1-propanol on cellulose tribenzoate. Under the term ''mass transfer kinetics'' or ''overall mass transfer kinetics'', we understand, both in this previous report [3] and, in this paper, the sole mass transfer resistance to the passage from the bulk mobile phase stream to the external surface of the particles and the diffusional mass transfer resistance inside the particles. We assume that the kinetics of surface adsorption–desorption is infinitely fast.

We showed [3] that the isotherm model that most accurately describes the adsorption behavior of the two enantiomers is the Tóth model [4–6]:

$$q_i = \frac{q_s K_i C_i}{[1 + (K_1 C_1 + K_2 C_2)^{\nu}]^{1/\nu}} \quad i = 1,2 \qquad (1)$$

where q_s is the saturation capacity of the monolayer, q_i and C_i are the concentrations of component i in the solid and the fluid phase at equilibrium, respectively, K_i is the equilibrium constant of component i, and ν is the heterogeneity parameter. In order to obtain a thermodynamically consistent model, the same saturation capacity must be assumed for both components. In writing this model (Eq. (1)), we also assumed that the heterogeneity parameter, ν, is the same for both enantiomers, which means that the chiral stationary phase (CSP) is equally heterogeneous with respect to both enantiomers. The best estimates of the parameters of the Tóth model (Eq. (1)) are reported in Table 1 [3]. Fig. 1 compares the experimental data regarding the competitive adsorption of the two enantiomers (symbols) and the best model isotherms (solid lines) calculated by fitting these experimental data to the Tóth isotherm equation. Note that the experimental data were measured for the racemic mixture only.

Table 1
Best estimates of the parameters for the Tóth model

Isotherm type	Parameters
Tóth	$q_s = 71 \pm 11$ $K_1 = 0.061 \pm 0.008$ $K_2 = 0.078 \pm 0.001$ $\nu = 0.77 \pm 0.06$

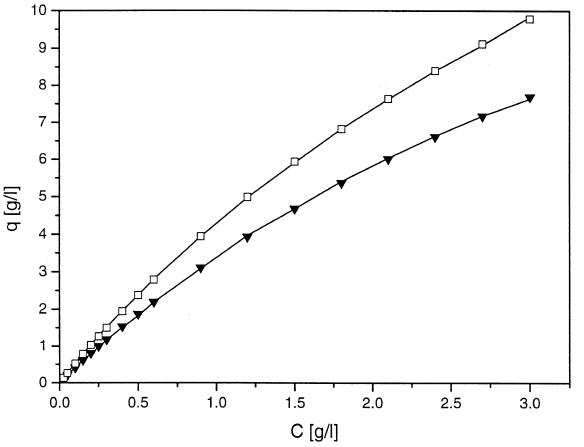

Fig. 1. Competitive adsorption of 1-phenyl-1-propanol on cellulose tribenzoate. Experimental data (symbols) and best theoretical isotherms (solid lines) calculated by means of Toth isotherm. Symbols: (□) S-PP; (▼) R-PP.

The agreement between the experimental data and the Tóth isotherm is excellent. This model, however, is significantly different from the conventional bilangmuir model that accounts often for the adsorption behavior of enantiomers on chiral phases [7]. The Tóth isotherm model assumes an heterogeneous surface while the bilangmuir model considers that the surface of the adsorbent contains two different types of sites, one that exhibits chiral selectivity, the other that does not, both surfaces being homogeneous.

The validity of the Tóth isotherm was demonstrated by comparing experimental peak profiles recorded for samples of the racemic mixture and the profiles calculated using the general rate model (GR) of chromatography [3] coupled with a Fickian pore diffusion model. The retention times and the peak shapes were well predicted.

However, this result could be obtained only by using different values of the pore diffusion coefficient under different experimental conditions.

The best values of the effective pore diffusion coefficient, $D_{eff} = D_{m,p}\varepsilon_p/\gamma$ (with $D_{m,p}$, pore molecular diffusion; ε_p, particle porosity; γ, tortuosity parameter), obtained in the earlier work [3] are reported in Table 2. These values were determined by fitting the experimental profiles to the profiles calculated with the GR model under different ex-

Table 2
Coefficients of pore diffusion, $D_{m,p}$[a], and effective diffusion, D_{eff}

$D_{m,p}$ (cm^2/min)		D_{eff} (cm^2/min)		Experimental conditions		
R-PP	S-PP	R-PP	S-PP	C_{tot} (g/l)	V_{inj} (ml)	L_f (%)
1.0×10^{-4}	1.0×10^{-4}	1.5×10^{-5}	1.5×10^{-5}	0.6	2	0.37
0.90×10^{-4}	1.0×10^{-4}	1.4×10^{-5}	1.5×10^{-5}	1.5	2	0.89
0.90×10^{-4}	1.0×10^{-4}	1.4×10^{-5}	1.5×10^{-5}	3	2	1.87
0.77×10^{-4}	1.3×10^{-4}	1.2×10^{-5}	2.0×10^{-5}	3	4	3.75
0.77×10^{-4}	1.3×10^{-4}	1.2×10^{-5}	2.0×10^{-5}	6	2	3.75

[a] C_{tot}, racemate concentration; V_{inj}, volume injected; L_f, column loading factor (ratio of the sample size to the monolayer capacity of the CSP in the column).

perimental conditions. Note that the pore molecular diffusion is at least 10 times smaller than the bulk molecular diffusion (see later, Table 3). This suggests that either pore hindrance is much greater than predicted by the classical equation for the tortuosity parameter or surface diffusion plays a dominant role in mass transfer inside the particles. As shown by the data reported in Table 2, the value of the effective pore diffusion coefficient decreases for R-PP and increases for S-PP with increasing concentration and volume of the sample of racemic mixture injected into the column.

Such a dependence of the effective pore diffusion on the concentration of the compounds investigated cannot be explained simply by a physico-chemical phenomenon. This result shows that pure intraparticle Fickian molecular diffusion is not a realistic assumption. The variation of the effective pore diffusion coefficient with the sample concentration in the mobile phase confirms that surface diffusion is the main contribution to the total diffusional flux.

The role of surface diffusion in the overall mass transfer between the bulk mobile phase and the interior of the particles of packing materials in reversed-phase liquid chromatography and the numerous investigations of this important phenomenon were recently reviewed [8]. However, all these previous studies were based on experimental data acquired in single-component chromatography. The methods described in these papers cannot be used to explain the opposite behavior observed for the effective diffusion coefficients of the two enantiomers of 1-phenol-1-propanol. Another possible approach is the use of the generalized Maxwell–Stefan equation that describes the surface diffusion flux. The aim of this work is to investigate the possibility of applying the GR model coupled with this equation for the modeling of enantiomeric separations.

2. Theory

2.1. General rate model of chromatography (GR)

In writing the equations of this model, we make the following assumptions:

1 the multicomponent fixed-bed process is isothermal;
2 the velocity of the moving phase is constant (its compressibility is negligible);
3 the bed is packed with particles of a porous adsorbent that are spherical and uniform in size;
4 the concentration gradient in the radial direction of the bed is negligible;
5 local equilibrium exists for each component between the pore surface and the stagnant fluid phase in the macropores;
6 the dispersion coefficient is constant;
7 external mass transfer resistances are negligible (see comments later).

With these assumptions, the following GR model, similar to the one discussed previously [5,6,9,10], can be formulated:

(a) Mass balance of the ith component in the mobile fluid phase:

$$\varepsilon_e\frac{\partial C_i}{\partial t}+u\frac{\partial C_i}{\partial z}=\varepsilon_e D_L\frac{\partial^2 C_i}{\partial z^2}-(1-\varepsilon_e)\frac{\partial \overline{C}_{p,i}}{\partial t} \quad (2)$$

where

$$\overline{C}_{p,i} = \frac{3}{R_p^3}\left[\int_0^{R_p} \varepsilon_p C_{p,i} r^2\, dr + \int_0^{R_p} (1-\varepsilon_p) q_i r^2\, dr\right] \quad (3)$$

(b) Mass balance of the ith component in the solid-phase:

$$\varepsilon_p \frac{\partial C_{p,i}}{\partial t} + (1-\varepsilon_p)\frac{\partial q_i}{\partial t} + \frac{1}{r^2}\frac{\partial}{\partial r}(r^2 J_{T,i}) = 0 \quad (4)$$

The diffusional flux, $J_{T,i}$, is given by

$$J_{T,i} = \varepsilon_p^* J_{m,i} + (1-\varepsilon_p)^* J_{s,i} \quad (5)$$

where $J_{m,i}$ is the molecular diffusion flux and $J_{s,i}$ the surface diffusion flux. The values of these flux will be discussed later, in connection with the application of the generalized Maxwell–Stefan equations (next section). In Eq. (5), we assumed parallel contributions of molecular and surface diffusion to the diffusion flux. Because the ratio of the cross-section area of the pores at a distance r to the surface of the sphere of radius r is equal to ε_p, the effective molecular flux is equal to $J_{m,i} \times \varepsilon_p$. A similar explanation is valid for the surface flux because it is referenced to the solid-phase.

(c) Initial conditions. For $t=0$, we have

$$C_i(0,z) = C_i^0 \quad (6)$$

for the first mass balance equation and for the second, for $0<z<L$ and $0<r<R_p$, we have

$$C_{p,i}(0,r,z) = C_{p,i}^0(r,z);\ q_i(0,r,z) = q_i^0(r,z) \quad (7)$$

(d) Boundary conditions for the first mass balance equation (Eq. 2). For $t>0$, at $z=0$, we have:

$$u_f C'_{fi} - u(0)C(0) = -\varepsilon_e D_L \frac{\partial C_i}{\partial z}$$

with

$$C'_{fi} = C_{fi} \quad \text{for} \quad 0<t<t_p$$
$$C'_{fi} = 0 \quad \text{for} \quad t_p<t \quad (8)$$

and for $t>0$, at $z=L$, we have:

$$\frac{\partial C_i}{\partial z} = 0 \quad (9)$$

(e) Boundary conditions for the second mass balance equation (Eq. 4). For $t>0$, at $r=R_p$, we have:

$$C_{p,i}(t,r) = C_i \quad (10)$$

and for $t>0$, at $r=0$, we have:

$$\frac{\partial C_{p,i}(t,r)}{\partial z} = 0 \quad (11)$$

Eqs. (2)–(11), together with the suitable isotherm model, constitute the GR model. This model is still incomplete, however. We must find a relationship expressing the diffusion flux inside the particles. In the present study, the initial concentration in the mobile and the stationary phase was assumed to be 0.

2.2. The diffusion flux and the generalized Maxwell–Stefan (GMS) equations

The total diffusion flux of a compound inside an adsorbent particle is the sum of the molecular and the surface diffusion flux, $J_{m,i}$ and $J_{s,i}$, respectively. Under the experimental conditions typically used in HPLC and particularly in chiral separations, the fluid concentrations of the components separated remain small (see Fig. 1).

Accordingly, we may assume that part of the diffusion flux connected with molecular diffusion, $J_{m,i}$, in the fluid impregnating the pores can be described by Fick equation:

$$J_{m,i} = -\frac{D_{m,i}}{\gamma}\frac{\partial C_{p,i}}{\partial r} \quad (12)$$

This is the model that was used previously [3]. In this model, the external mass transfer resistance was ignored because it was shown to have a negligible influence on band broadening and on peak profiles in the chromatographic system investigated. However, the observation reported earlier that a good agreement between the experimental profiles of the two bands recorded for the racemic mixture and those calculated with the GR model could be achieved only by using values of the effective diffusion coefficients of the two enantiomers that depend on their concentration suggested that a more complex but more correct model of diffusion flux inside the particles should be used.

The dependency of intraparticle mass transfer on the concentration can be explained by assuming that surface diffusion plays a dominant role in the overall mass transfer kinetics. We investigated how two different surface diffusion models can account for the effect observed. The difference between these two models is discussed in Appendix A. In each model, the surface diffusion flux is calculated using the following two equations.

$$J_{s,1} = -\left(D_{s,11}\frac{\partial C_{p,1}}{\partial r} + D_{s,12}\frac{\partial C_{p,2}}{\partial r}\right) \quad (13)$$

$$J_{s,2} = -\left(D_{s,21}\frac{\partial C_{p,1}}{\partial r} + D_{s,22}\frac{\partial C_{p,2}}{\partial r}\right) \quad (14)$$

These equations can be derived by assuming that the surface chemical potential gradient is the driving force of surface diffusion, see Krishna [11] and the discussion presented by Karger and Ruthven [12]. The coefficients $D_{s,ij}$ in these equations are the Fickian diffusivities of the generalized Maxwell–Stefan equations (GMS). According to the formulation of the Maxwell–Stefan model, these coefficients are given by one of the following sets of equations (see Appendix A).

$$D_{s,11} = \frac{q_1}{C_{p,1}} D_1[\theta_1 D_2 + D_{1,2}]/[\theta_1 D_2 + \theta_2 D_1 + D_{1,2}] \quad (15)$$

$$D_{s,12} = \frac{q_2}{C_{p,2}} \theta_1 D_2 D_1/[\theta_1 D_2 + \theta_2 D_1 + D_{1,2}] \quad (16)$$

$$D_{s,21} = \frac{q_1}{C_{p,1}} \theta_2 D_1 D_2/[\theta_1 D_2 + \theta_2 D_1 + D_{1,2}] \quad (17)$$

$$D_{s,22} = \frac{q_2}{C_{p,2}} D_2[\theta_2 D_1 + D_{1,2}]/[\theta_1 D_2 + \theta_2 D_1 + D_{1,2}] \quad (18)$$

or

$$D_{s,11} = \frac{q_1}{C_{p,1}} D_{1,\nu}[\theta_1(D_{2,\nu} - D_{1,2}) + D_{1,2}]/ [\theta_1(D_{2,\nu} - D_{1,2}) + \theta_2(D_{1,\nu} - D_{1,2}) + D_{1,2}] \quad (15a)$$

$$D_{s,12} = \frac{q_2}{C_{p,2}} \theta_1 D_{2,\nu}(D_{1,\nu} - D_{1,2})/[\theta_1(D_{2,\nu} - D_{1,2}) + \theta_2(D_{1,\nu} - D_{1,2}) + D_{1,2}] \quad (16a)$$

$$D_{s,21} = \frac{q_1}{C_{p,1}} \theta_2 D_{1,\nu}(D_{2,\nu} - D_{1,2})/[\theta_1(D_{2,\nu} - D_{1,2}) + \theta_2(D_{1,\nu} - D_{1,2}) + D_{1,2}] \quad (17a)$$

$$D_{s,22} = \frac{q_2}{C_{p,2}} D_{2,\nu}[\theta_2(D_{1,\nu} - D_{1,2}) + D_{1,2}]/ [\theta_1(D_{2,\nu} - D_{1,2}) + \theta_2(D_{1,\nu} - D_{1,2}) + D_{1,2}] \quad (18a)$$

The coefficients D_{ij} are the GMS diffusion coefficients for counter-sorption diffusivity of the two species, 1 and 2. The coefficients D_i in the first model (Eqs. (15)–(18)), describe the interactions between the sorbent species and the adsorbent. The coefficients $D_{i,\nu}$, in the second model (Eqs. (15a)–(18a)), are the GMS diffusion coefficients that reflect the facility of the exchange between the sorbed species i and the vacant sites, and θ_i is the fractional surface coverage of species i.

2.3. Methods used for the calculation of numerical solutions of the model

The GR model was solved by numerical calculations, using a program based on the method of orthogonal collocation on finite elements [5,6,13,14]. The set of discretized ordinary differential equations obtained in this method was solved with the Adams–Moulton method implemented following the VODE procedure [15]. The relative (RTOL) and absolute (ATOL) tolerance parameters used to control the error in concentration calculation were equal to 10^{-6} and 10^{-8}, respectively. The estimated local error on Y(i), EWT(i), will be controlled so as to be roughly less than

$$\begin{aligned} &\mathrm{EWT}(i) = \mathrm{RTOL}^*|\mathrm{Y}(i)| + \mathrm{ATOL} \quad \text{if} \quad \mathrm{ITOL} = 1, \text{ or} \\ &\mathrm{EWT}(i) = \mathrm{RTOL}^*|\mathrm{Y}(i)| + \mathrm{ATOL}(i) \quad \text{if} \quad \mathrm{ITOL} = 2. \end{aligned} \quad (19)$$

Thus, the local error test is passed if, for each component, either the absolute error is less than ATOL or ATOL(i), or the relative error is less than

RTOL. The actual global errors may exceed these local tolerances, so they should be chosen conservatively.

The integrals in Eq. (3) were calculated using the method of Gauss quadrature [14].

3. Experimental

Complete details regarding the experimental work can be found in a previous publication [3]. We report here only the most important experimental conditions.

3.1. Equipment

A HP 1090 instrument for liquid chromatography (Hewlett-Packard, Palo Alto, CA, USA) was used for all the experimental determinations. This system is equipped with a multi-solvent delivery system, an automatic sample injector with a 25-μl loop, a diode-array detector, and a computer for data acquisition. A back pressure regulator (100 p.s.i., Upchurch, Scientific Oak Arbor, WA, USA) was inserted downstream the detector unit.

3.2. Materials

3.2.1. Mobile phase and chemicals

The mobile phase was a 97:3 (v/v) mixture of *n*-hexane and 2-propanol. Both hexane and 2-propanol were HPLC-grade solvents from Fisher Scientific (Fair Lawn, NJ, USA).

The column hold-up volume was measured with 1,3,5-tri-*tert*.-butylbenzene, purchased from Aldrich (Milwaukee, WI, USA). The racemic mixture of 1-phenyl-1-propanol was also from Aldrich. It had been previously purified in our laboratory [16].

3.2.2. Column

A 20×1.0-cm stainless steel column was packed in our laboratory [16] with Chiralcel OB (cellulose tribenzoate coated on porous silica, Daicel, Tokyo, Japan). This column was used for all the experiments. The average particle diameter of this packing material is 20 μm. The total column porosity, measured by injecting 1,3,5-tri-*tert*.-butylbenzene, a compound that can be considered as unretained on this column [16,17], was 0.715.

3.2.3. Procedures for isotherm determination

All the experimental data were acquired at room temperature (22.5–24.5 °C), using the racemic mixture, and with a mobile phase flow-rate of 2.0 ml/min. The experimental reproducibility of the retention times, which constitutes the primary raw data, was around 1%. The competitive isotherm data were measured by frontal analysis (FA) at $\lambda = 280$ nm. The same λ value was used for the recording of the overloaded profiles. The detector was calibrated several times during the experimental work and every times overloaded profiles were recorded. The calibration curve was not linear, although work was done in a relatively low concentration range. It was approximated by a cubic spline. Reproducibility between different calibration curves was approximately 3–5%.

All measurements were made in triplicate. The isotherm data were calculated by averaging the results.

The experimental parameters used in the GR model are given in Table 3. All the calculations performed for this work used the following values of the GMS diffusion coefficients, $D_{1,v} = 7.9 \times 10^{-6}$ cm^2/min, $D_{2,v} = 8 \times 10^{-6}$ cm^2/min, and $D_{1,2} = D_{2,1} = 1 \times 10^{-5}$ cm^2/min. These values of these diffusion coefficients were estimated in such a manner as to achieve the best possible agreement between the experimental and the calculated band profiles.

Table 3
GR models parameters

Parameter	Value
Molecular bulk phase diffusion coefficient, D_m (cm^2/min)	0.0017
Dispersion coefficient, D_L (cm^2/min)	0.0032
Total porosity, ε_t	0.715
External porosity, ε_e	0.35
Internal porosity, ε_p	0.561

4. Results and discussion

4.1. Validation of the GR–GMS Model

There are five unknown parameters in the diffusional flux models described by Eqs. (5), (12), and (15)–(18) or (15a)–(18a), two molecular diffusion coefficients and three surface diffusion coefficients. However, as explained earlier, surface diffusion plays the dominant role and, as a first approximation, we neglected the molecular diffusion flux.

The only adjustment made was in the selection of the best values of the GMS diffusion coefficients, defined as those minimize the discrepancies between the two sets of band profiles, those measured and those calculated. The best agreement between measured and calculated data, illustrated in Figs. 2–6, is obtained for the Fickian diffusivities derived from Eqs. (15a)–(18a), despite the fact that Eqs. (15a)–(18a) were developed under the assumption of equivalence of the vacancies (see Appendix A), an assumption that is not strictly fulfilled in our case because we proved that the adsorbent surface is heterogeneous (the isotherm data are accounted for by the Tóth model). A slightly less good agreement, not presented here, was obtained when the Fickian diffusivities were derived from the more physically correct Eqs. (15)–(18) (see Appendix A).

By contrast with what had to be done in our earlier work [3], the same values of the diffusion coefficients were used in the five different experimental cases illustrated in Figs. 2–6. The kinetic parameters no longer depend on the concentration of the studied compounds and this is an important result. In a second approach, we tried to describe the peaks profile more accurately by taking into consideration also the molecular diffusion flux. We checked that the molecular flux, given by Eq. (12), has a negligible impact on the total molecular flux, given by Eq. (5), when the pore molecular diffusion is smaller than about 2×10^{-6} (cm^2/min). For greater values of

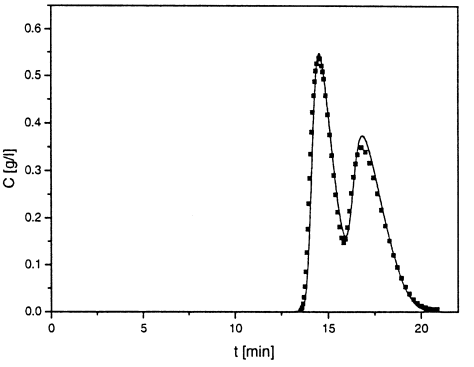

Fig. 3. Comparison between the experimental band profiles (symbols) and the numerical solution (solid lines) of the GR-GMS model. Total concentration of racemic mixture: $C=1.5$ g/l. Injection volume 2 ml, $L_f=0.89\%$.

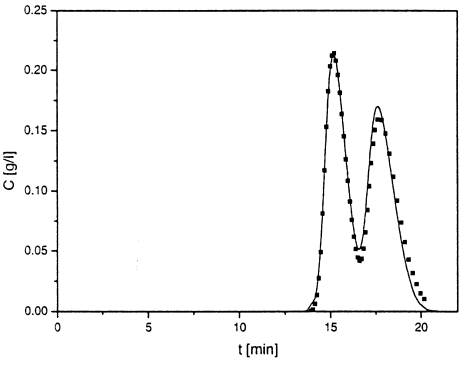

Fig. 2. Comparison between the experimental band profiles (symbols) and the numerical solution (solid lines) of the GR-GMS model. Total concentration of racemic mixture: $C=0.6$ g/l. Injection volume 2 ml, $L_f=0.37\%$.

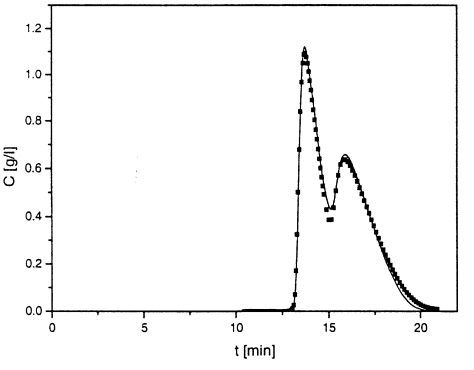

Fig. 4. Comparison between the experimental band profiles (symbols) and the numerical solution (solid lines) of the GR-GMS model. Total concentration of racemic mixture: $C=3$ g/l. Injection volume 2 ml, $L_f=1.87\%$.

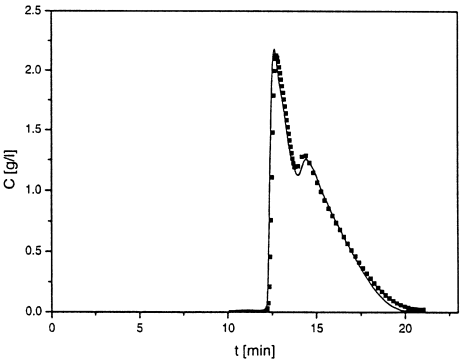

Fig. 5. Comparison between the experimental band profiles (symbols) and the best numerical solution (solid lines) of the GR-GMS model. Total concentration of racemic mixture: $C=6$ g/l. Injection volume 2 ml, $L_f=3.75\%$.

the pore molecular diffusivity, we were not able to choose values of the surface diffusion coefficients in such way as to obtain a better agreement of the calculated profiles with the experimental ones than the one achieved when the pore diffusion flux was ignored.

A detailed comparison of sets of experimental profiles and profiles calculated with the GR-GMS model is shown in Figs. 2–6. A better agreement between calculated and experimental profiles is obtained for the first than for the second enantiomer. The height of the first eluted peak, that of S-PP, is slightly too low at low concentrations and slightly too large at the highest concentration, but by only a few percent. The opposite trend is observed for the second component. However, in this discussion, we must also take into account the fact that the racemic mixture of 1-phenyl-1-propanol that we used was contaminated by a small amount of an unidentified impurity that elutes on the rear of the band of the second component (not showed on the figures) and may affect, to a small extent, the corresponding part of this profile. Accordingly, we may conclude that the GR model coupled with the GMS equations does correctly describe the experimental peak profiles in a case in which the mass transfer kinetics is not very fast.

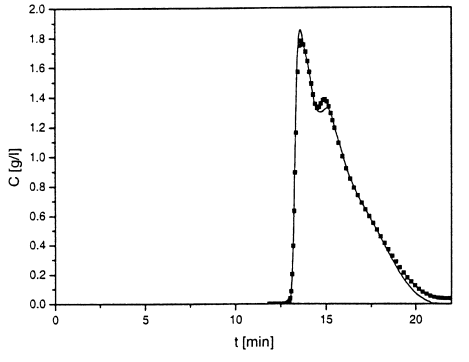

Fig. 6. Comparison between the experimental band profiles (symbols) and the best numerical solution (solid line) of the GR-GMS model. Total concentration of racemic mixture: $C=3$ g/l. Injection volume 4 ml, $L_f=3.75\%$.

4.2. Influence of counter-sorption diffusivity ($D_{1,2}$) on the band profiles

The GMS model introduces a new parameter, the coefficient of counter-sorption diffusion, $D_{1,2.}$ The influence of this coefficient on the band profiles of the two enantiomers is illustrated in Fig. 7. Calculations of the elution profile of a large sample of the racemic mixture were performed for the following values of $D_{1,2}$, 5×10^{-7}, 1×10^{-6}, 5×10^{-6}, 1×10^{-5}, and 2×10^{-5} cm^2/min, using the Fickian diffusivities defined by Eqs. (15a)–(18a). The results of the numerical calculation are shown in Fig. 7.

We observe that when the counter-sorption diffusivity increases from $D_{1,2}=5\times10^{-7}$ to $D_{1,2}=1\times$

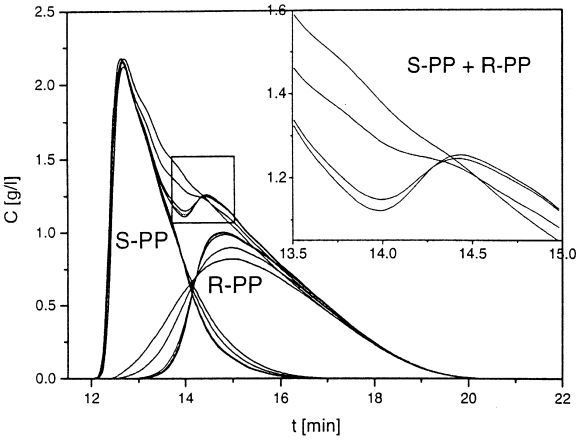

Fig. 7. Influence of the counter-sorption diffusion coefficient, $D_{1,2}$, on the band profiles of the enantiomers of 1-phenol-1-propanol. Total concentration of the racemic mixture: $C=6$ g/l. Injection volume 2 ml, $L_f=3.75\%$.

10^{-5} cm^2/min, the height of the band of the R-PP enantiomer (the second one eluted) increases and the separation of the two enantiomers improves (a valley appears between the two bands). Other calculations (results not shown), however, demonstrate that the value of this diffusion coefficient has only a minor influence on the profile of the band of the R-PP enantiomer when $D_{1,2}$ becomes greater than about 1×10^{-5} cm^2/min.

By contrast, in all cases, the counter-sorption diffusivity has a nearly negligible influence on the band profile of the band of S-PP, especially in the vicinity of its front shock and its apex. There is only a very slight influence on the band tail (see Fig. 7).

This observation is easily explained by the model. In the front of the elution band of the first eluted enantiomer, S-PP, the concentration of the second enantiomer, R-PP, is zero. Then, Eqs. (13) and (14) show that the total diffusion flux of S-PP is the same as for a band of pure S-PP and does not practically depend on the value of the counter-sorption diffusivity. On the other hand, in the mixed zone between the two bands and particularly in the area of the front shock of the second enantiomer, there is a strong effect of counter-current diffusion in the adsorbent particle. The S-PP enantiomer is diffusing out of the particle while the R-PP enantiomer is diffusing into it. The effective diffusion flux of R-PP through the particle is strongly influenced by the diffusion flux of S-PP in the opposite direction.

4.3. Conclusion

This work demonstrates that the combination of the GR model with the GMS equations provides a powerful approach to account for the profiles of the elution bands of multicomponent mixtures in liquid chromatography when the mass transfer kinetics is relatively slow, a common occurrence in chiral separations. Application of this model provided an excellent agreement between the experimental and calculated band profiles. This new model could be applied to many other similar separations and possibly to protein separations as well.

The new model described here accounts also for an observation sometimes made that the separation between two bands appears more difficult to achieve than could be predicted on the basis of the equilibrium thermodynamics and assuming that the mass transfer kinetics of the two components in the phase system are independent of their concentrations and independent of the presence of the other components of the mixture to separate. Our results also confirm the suggestions presented in many earlier papers that surface diffusion plays an important if not a dominant role in the resistances to mass transfer from the bulk phase to the interior of the packing particles. It seems only that the actual situation might be more complicated than previously expected and that the mass transfer kinetics may be competitive.

4.4. Nomenclature

C	concentration in mobile phase
C_p	concentration in the stagnant fluid phase contained inside pores
D_L	dispersion coefficient
D_m	molecular diffusion coefficient
D_{eff}	effective (or inside-pore) diffusion coefficient
J_T, J_m, J_s	total, molecular and surface flux
K	equilibrium constant
L	column length
q	concentration in the solid-phase
q_s	saturation capacity
r	radial coordinate
R_p	particle radius
t	time
t_p	injection time
u	linear velocity
z	axial coordinate
Greek letters	
γ	tortuosity parameter
ε_e	external porosity
ε_p	internal (pore) porosity
ε_t	total porosity
ν	heterogeneity parameter
Θ_i	fractional surface occupancy of species i
Subscripts	
i,j	component index or site index
f	inlet value
Superscripts	
0	initial value
$\bar{}$	average value

Acknowledgements

This work was supported in part by grant CHE-00-70548 of the National Science Foundation and by the cooperative agreement between the University of Tennessee and the Oak Ridge National Laboratory.

Appendix A

A.1. Generalized Maxwell–Stefan (GMS) diffusion model

A detailed description of the derivation of the Maxwell–Stefan relationships was given by Taylor and Krishna [18]. The application of the Generalized Maxwell–Stefan equations to the description of the multicomponent surface diffusion of adsorbed species and the derivation of the equations reported in the main text (Eqs. (13)–(18) and (15a)–(18a)) was discussed earlier [11,12,19–23]. For the convenience of the readers, a brief description of this derivation is given below.

Originally the GMS approach was used to investigate gas adsorption on zeolites. We assumed arbitrarily here that this equation can also be used for the modeling of surface diffusion in the mesopores of the silica particles of the packing materials used in liquid chromatography.

(a) Development of Eqs. (13–18).

Krishna [19–22] extended the dusty gas model [24] approach to the description of surface diffusion of adsorbed molecules starting from Eq. (A.1) for *n*-component mixture:

$$-\frac{\Theta_i}{RT}\nabla\mu_i = \sum_{\substack{j=1 \\ j\neq i}} \frac{\Theta_j J_{s,i} - \Theta_i J_{s,j}}{q_s D_{ij}} + \frac{J_{s,i}}{q_s D_i} \tag{A.1}$$

where $\Theta_i = q_i/q_s$ is the fractional surface occupancy of species i; $\nabla\mu_i$ is the surface chemical potential gradient of species i at constant temperature and spreading pressure; R is the universal gas constant; T is the temperature; q_s is the saturation capacity of the adsorbent; D_{ij} are the GMS counter-sorption diffusivity coefficients; D_i is called the corrected diffusivity [5] or the Maxwell–Stefan diffusivity describing the interaction between component i and the adsorbent [19–23].

Assuming that equilibrium prevails between the adsorbed species and the bulk fluid, the surface chemical potential of species i can be expressed as:

$$\mu_i = \mu_i^0 + RT \ln f_i \tag{A.2}$$

where f_i is the fugacity of component i in the bulk fluid phase in equilibrium with the sorbent. For one-dimensional transport along the particle radius, the driving force on the left-hand side of Eq. (A.1) can be rewritten in terms of the gradient of fractional coverage:

$$\frac{\theta_i}{RT}\nabla\mu_i = \frac{\theta_i}{RT}\sum_{j=1}^{n}\frac{\partial\mu_i}{\partial\theta_j}\frac{\partial\theta_j}{\partial r} = \theta_i\sum_{j=1}\frac{\partial \ln f_i}{\partial\theta_j}\frac{\partial\theta_j}{\partial r} = \sum_{j=1}^{n}\Gamma_{ij}\frac{\partial\theta_j}{\partial r} \tag{A.3}$$

where $\underline{\Gamma}$ is an n-dimensional matrix having as elements:

$$\Gamma_{ij} = \theta_i\frac{\partial \ln f_i}{\partial\theta_j} \tag{A.4}$$

The surface diffusivities D_{ij} defined in Eq. (A.1) are the GMS counter-sorption diffusivities. Counter-sorption takes place when components i and j exchange positions on the adsorbent surface. The counter-sorption of two species has a greater probability of occurrence at high surface coverage. The Onsager reciprocal relations shows that these coefficients are symmetrical, e.g., that $D_{ij} = D_{ji}$ [11].

From Eq. (A.1) the surface fluxes can be derived:

$$\underline{J_s} = -q_s\underline{\underline{B}}^{-1}\underline{\Gamma}\frac{\partial\underline{\theta}}{\partial r} \tag{A.5}$$

where $\underline{J}$ is the column vector of the surface diffusion fluxes, $\underline{\theta}$ is the column vector of the fractional coverage of the different species involved. The matrix $\underline{B}$ for two component mixture, investigated in this work, is defined as follows:

$$\underline{\underline{B}} = \begin{bmatrix} \frac{1}{D_1} + \frac{\theta_2}{D_{12}} & -\frac{\theta_1}{D_{12}} \\ -\frac{\theta_2}{D_{12}} & \frac{1}{D_2} + \frac{\theta_1}{D_{12}} \end{bmatrix} \tag{A.6}$$

In the following, we assumed that the mobile phase

is ideal, so the fugacity, f_i, of the mobile phase can be replaced by its concentration $C_{p,i}$.

Combining Eqs. (A.4) and (A.6) with Eq. (A.5) and remembering that:

$$\frac{\partial C_{p,i}}{\partial r} = \sum_{j=1}^{n} \frac{\partial C_{p,i}}{\partial \Theta_j} \frac{\partial \Theta_j}{\partial r} \tag{A.7}$$

one can derive Eqs. (13) and (14) with the Fickian diffusivities defined by Eqs. (15)–(18).

A more complex GMS diffusion model for multicomponent surface diffusion was formulated by Krishna under the following assumptions [11]:

1 equilibrium prevails between the adsorbed species and the bulk fluid,
2 the vacant sites on the adsorbent surface can be considered as the $(n+1)$th component of the system,
3 all the vacant sites are equivalent.

In the GMS model, the surface-diffusion flux in the $(n+1)$-component system consisting of the n sorbed species and the vacant sites is written in a manner analogous to that of diffusion in bulk fluid phases [11,18], as:

$$-\frac{\Theta_i}{RT}\nabla\mu_i = \sum_{\substack{j=1 \\ j\neq i}} \frac{\Theta_j J_{s,i} - \Theta_i J_{s,j}}{q_s D_{ij}} + \frac{\Theta_\nu J_{s,i} - \Theta_i J_{s,\nu}}{q_s D_{i,\nu}} \tag{A.8}$$

The coefficient $D_{i,v}$, reflects the facility of the exchange between the sorbed species i and the vacant sites.

The same mathematical manipulations as above permit the derivation of Eqs. (13)–(14) and Eqs. (15a)–(18a) giving the surface fluxes, from Eq. (A.8). We should notice, however, that, by applying the model consisting in Eqs. (13)–(14) and (15a)–(18a) to a heterogeneous surface, we violate the assumption (3) of the equivalence of the vacancies. In spite of this restriction, the GMS model described by equation (A.8) proved to be the best model of the kinetics of mass transfer for 1-phenol-1-propanol (see Section 4).

References

[1] S. Ahuja, in: Chiral Separations by Chromatography, Oxford University Press, Washington, DC, 2000.
[2] E.J. Ariens, Med. Res. Rev. 6 (1986) 451.
[3] A. Cavazzini, K. Kaczmarski, P. Szabelski, D. Zhou, X. Liu, G. Guiochon, Anal. Chem. 73 (2001) 5704.
[4] J. Tóth, Acta Chim. Acad. Sci. Hung. 69 (1971) 311.
[5] D.M. Ruthven, in: Principles of Adsorption and Adsorption Processes, Wiley, New York, 1984.
[6] G. Guiochon, S.G. Shirazi, A.M. Katti, in: Fundamentals of Preparative and Nonlinear Chromatography, Academic Press, Boston, MA, 1994.
[7] T. Fornstedt, P. Sajonz, G. Guiochon, Chirality 10 (1998) 375.
[8] K. Miyabe, G. Guiochon, Adv. Chromatogr. 40 (2000) 1.
[9] M. Suzuki, in: Adsorption Engineering, Elsevier, Amsterdam, 1990.
[10] G.A. Heeter, A.I. Liapis, J. Chromatogr. A 796 (1998) 157.
[11] R. Krishna, Chem. Eng. Sci. 45 (1990) 1779.
[12] J. Karger, D.M. Ruthven, in: Diffusion in Zeolites and other Microporous Solids, Wiley, New York, 1992.
[13] K. Kaczmarski, G. Storti, M. Mazzotti, M. Morbidelli, Comput. Chem. Eng. 21 (1997) 641.
[14] V.J. Villadsen, M.L. Michelsen, in: Solution of Differential Equation Model by Polynomial Approximation, Prentice-Hall, Englewood Cliffs, NJ, 1978.
[15] P.N. Brown, A.C. Hindmarsh, G.D. Byrne, Ordinary Differential Equation Solver—procedure, available at http://www.netlib.org
[16] S. Khattabi, D.E. Cherrack, J. Fisher, P. Jandera, G. Guiochon, J. Chromatogr. A 877 (2000) 95.
[17] F. Charton, S.C. Jacobson, G. Guiochon, J. Chromatogr. 630 (1993) 21.
[18] R. Taylor, R. Krishna, in: Multicomponent Mass Transfer, Wiley, New York, 1993.
[19] R. Krishna, Gas Sep. Purif. 7 (1993) 91.
[20] R. Krishna, Chem. Eng. Sci. 48 (1993) 845.
[21] R. Krishna, T.J.H. Vlugt, B. Smit, Chem. Eng. Sci. 54 (1999) 1751.
[22] R. Krishna, Chem. Phys. Lett. 326 (2000) 477.
[23] F. Kapteijn, J.A. Moulijn, R. Krishna, Chem. Eng. Sci. 55 (2000) 2923.
[24] E.A. Mason, A.P. Malinauskas, in: Gas Transport in Porous Media: The Dusty Gas Model, Elsevier, Amsterdam, 1983.